Effect of Cation Exchange Capacity on the Structure and Dynamics of Poly(ethylene oxide) in Li^+ Montmorillonite Nanocomposites

V. KUPPA,[1] E. MANIAS[2]

[1]Department of Chemical Engineering, Massachusetts Institute of Technology, Cambridge, Massachusetts 02139

[2]Department of Materials Science and Engineering, Pennsylvania State University, University Park, Pennsylvania 16802

Received 2 May 2005; revised 11 July 2005; accepted 21 July 2005
DOI: 10.1002/polb.20644
Published online in Wiley InterScience (www.interscience.wiley.com).

ABSTRACT: Molecular dynamics computer simulations are used to study the structure and dynamics of 1-nm wide films of poly(ethylene oxide) (PEO) confined between mica-type layered silicates of different cation exchange capacities (CEC). The simulation setup mimics experimental systems formed by intercalation of PEO in montmorillonite alumino-silicates with varied inherent charges. It is shown that the presence and population of lithium has a significant influence on the behavior of the system, in addition to the confinement-induced effects caused by the extreme spatial restriction. The structural features of the confined PEO are strongly altered with the number of Li^+, which determines the polymer/inorganic interactions. The combination of the nanoconfinement and the presence of lithium preclude regular ordered arrangements of PEO, similar to those observed in the bulk unconfined polymer. The segmental dynamics of PEO in confinement are also greatly influenced by the presence of lithium, because of the strong interaction between Li^+ and the oxygen of the PEO backbone.
 J Polym Sci Part B: Polym Phys 43: 3460–3477, 2005
Keywords: molecular dynamics; nanoscopically confined polymers; polymer/inorganic nanocomposites; self-assembled nanostructures; simulations

INTRODUCTION

Polymer/layered-silicate intercalated nanocomposites have become an attractive class of systems to study the fundamentals of nanoscopically confined polymers.[1,2] One promising way to synthesize polymer nanocomposites is by direct intercalation of polymers in layered inorganic hosts.[3–6] Graphite, transition metal chalcogenides, metal phosphates, complex oxides, oxychlorides, and mica-type layered silicates are some examples of layered solids capable of intercalation. The structure and properties of the resulting nanocomposite can be conveniently mediated by controlling subtle guest–host interactions. In our study, the focus is on mica-type layered silicates in which the poly(ethylene oxide) (PEO) is confined in well-defined nanoscopically wide (0.87 nm) slits, which are formed by self assembly of negatively charged parallel stacks of the alumino-silicate layers.[3,7–10] These inorganic crystalline layers can be naturally occurring or synthetic and are typically 1-nm thick and several micrometer in lateral dimen-

Correspondence to: V. Kuppa (E-mail: kuppa@mit.edu) or E. Manias (E-mail: manias@psu.edu)

Journal of Polymer Science: Part B: Polymer Physics, Vol. 43, 3460–3477 (2005)

sions, bearing a native hydrated cation layer in the interlayer galleries. The thermodynamic driving force for the intercalation of PEO in such severe pseudo-two-dimensional geometries is due to the free energy gain of PEO replacing the water.[9–11] Where the Li^+ montmorillonite layers are used as the inorganic confining hosts, it is possible to systematically vary the surface density of the Li^+ cations (through cation exchange capacity (CEC) reduction approaches[12–14]) and for moderate reductions of the CEC, one can retain the favorable thermodynamics for PEO intercalation.[15]

The present molecular modeling approach parallels experimental investigations probing the fundamental physics and molecular dynamics of about 1-nm thick PEO/Li^+ films confined between montmorillonite clay platelets.[7–11,16] The focus of this study is on providing a better understanding of the segmental relaxations, chain dynamics, and the structural arrangement of these nanoconfined polymer layers, and in particular on connecting the confinement-induced behavior to the polymer/inorganic interactions (a connection that still remains elusive despite numerous experimental and simulations studies of such systems[1,7–11,16–19]).

Here, we perform a Molecular Dynamics simulation study of PEO intercalated in clays of different inherent charges (varied CEC montmorillonites), so as to comparatively explore the effects of geometric confinement and of varied polymer/inorganic interactions (realized through varying the number of counterbalancing lithium ions in the interlayer). We build on our previous work[18–20] aiming to further our insights into the molecular origins underlying the behavior of nanoconfined Li^+/PEO films, as it relates to both the structure and the dynamics of the polymer and the Li^+.

SIMULATION DETAILS

Method and Systems

Molecular Dynamics simulations of fully atomistic models of PEO hexamers intercalated between montmorillonite crystalline layers were performed. Complete details of the simulation method and the force fields employed are given elsewhere.[18] All systems were simulated for 5 ns each after equilibration, under NVT conditions, with a time step of 1 fs, and a weak coupling to a temperature bath realized via a Berendsen thermostat.[21] System trajectories were saved every 10 ps for postsimulation analyses. Bulk unconfined PEO systems were also simulated, albeit under NPT conditions and in the presence of smaller salt concentrations.[18,19]

Simulations were carried out for three different CECs of the confining silicate surfaces, varied by changing the partial charge of the octahedral aluminum layer, and adjusting the number of counter-balancing lithium cations in a commensurate manner to preserve electrostatic neutrality. This situation mimics the experimental systems formed by intercalation of PEO in reduced-CEC montmorillonites.[15] The different CECs that we studied here are 1.44, 1.05, and 0.64 mequiv/g, and correspond to 29, 21, and 13 Li^+ cations/montmorillonite layer, respectively, for our $3.696 \times 3.656 \times 3.558$ nm^3 simulation box.[22,23] Studies were also carried out on a fully neutral wall surface, that is, a system in which no counterbalancing cations are present and the inorganic surfaces bear no negative charge. For this last system, the z-size of the simulation box was slightly reduced so that the average PEO density in each slit becomes the same as those systems that include Li^+. It must be mentioned here that this last system is purely theoretical, since there is no driving force for intercalation of PEO in such nanometer confinements, as also evident by the inability to experimentally intercalate PEO in fully-neutralized montmorillonite[15] or in talc.[24] All systems studied, both intercalated and bulk, are completely "dry," that is, there is no water in any of the simulated systems. This is not obvious for the respective experimental systems—especially for the higher CEC silicates—that contain small amounts of "structural" water, which is very difficult to remove.[24] In most cases, traces of water remain inside the intercalated PEO structures, albeit in very small quantities, typically below the detection limit of solid-state NMR.[9,10] Simulations that account for the presence of water in PEO/montmorillonite intercalates have been reported earlier.[17]

In all intercalated structures, the lithium cations dictate the system interactions. Namely, beyond the interatomic van der Waals interatomic interactions, common across systems, the polymer/inorganic interactions are varied between systems by the number of Li^+ present. Specifically, these interactions are determined by the competitive coordination of montmorillonite and PEO oxygens to the Li^+; that is, the electrostatic attraction of Li^+ to the negative montmorillonite layers (Li^+ coordination with montmorillonite oxygens) balanced by the Li^+ coordination

to the PEO oxygens. This balance of interactions has shown to dictate both the lithium mobility,[18] as well as the PEO structure[20] and dynamics[19] in these nanoscopically confined systems.

Order Parameters

The simulations are performed on short oligomers formed by six ethylene oxide repeating units that cannot create extended crystalline arrangements characteristic of helical configuration of pure PEO. To examine the short range ordering of the polymer chains in our system, we turn to calculations of order parameters that can probe local periodicities over a few atoms. Namely, we compute translational, orientational, and rotationally invariant order parameters. The definitions and the physical significance of each parameter are analyzed in detail in our earlier work.[19] For completeness and self-consistency for this manuscript, they are also defined here.

1. The parameter of translational order (τ) is defined by:

$$\tau = \frac{\int_0^{\xi_c} |g(\xi) - 1| d\xi}{\xi_c} \quad (1)$$

where ξ is the normalized radial distance between carbon atoms ($\xi = r\rho^{1/3}$, where r is the carbon radial distance, ρ is the carbon number density); $g(\xi)$ is the interchain radial (pair) distribution function of the carbons in the simulation cell; ξ_c is a cutoff distance, whose value was chosen here as half of the smallest box dimension. $\langle \tau_i \rangle$ is thus a scalar parameter indicative of the stacking periodicity between adjacent chains, its value ranges between 0 and 1, with lower values reflecting no preferential spacing in the system (0 corresponds to an ideal gas[25]) and higher values indicating a higher system crystallinity (1 would be a perfect crystal structure[25]).

2. The parameter of orientational order (q) is defined in the manner proposed by Chau and Hardwick,[26] as follows:

$$q_i = 1 - \frac{3}{32} \sum_{j=1}^{3} \sum_{k=j+1}^{4} \left(\cos \Psi_{j,i,k} + \frac{1}{3} \right)^2 \quad (2)$$

where $\Psi_{j,i,k}$ scans all the angles centered on an oxygen atom i and defined by all pairs (j,k) of its four nearest interchain oxygen neighbors. The numerical factors used normalize the value for q between 0 and 1 (with 1 corresponding to a perfect tetrahedral arrangement centered around the i oxygen). In a first approximation, q quantifies how closely the orientation of four nearest interchain oxygens follows a perfect tetrahedral arrangement.

3. The third measure of structural ordering that we use is a rotationally invariant order parameter that was first defined by Steinhardt et al.[27] and ten Wolde et al.[28] in their studies of crystal nucleation. It serves as a generic crystallinity index, since it is independent of crystal symmetry and the orientation of the structure in space. It is calculated as follows: all the neighbors j of a particular particle i within a radius r_q are identified. The position vectors r_{ij} between neighbors are then normalized to unit vectors $\hat{r_{ij}}$ and their polar and azimuthal angles θ_{ij} and ϕ_{ij} are determined. The local structure around particle i is characterized by its order parameter $\bar{q}_{lm}$, which is constructed using the spherical harmonics $Y_{lm}(\theta_{ij},\phi_{ij}) = Y_{lm}(\bar{r}_{ij})$ and summing over all $N_b(i)$ neighbors of particle i:

$$\bar{q}_{lm}(i) = \frac{1}{N_b(i)} \sum_{j=1}^{N_b(i)} Y_{lm}(\hat{r}_{ij}) \quad \text{and}$$

$$\bar{Q}_{lm} = \frac{\sum_{i=1}^{N} N_b(i) \bar{q}_{lm}(i)}{\sum_{i=1}^{N} N_b(i)} \quad (3)$$

In this case, $\bar{q}_{lm}$ is a local order parameter, obtained for each i, whereas the global order parameter $\bar{Q}_{lm}$ is calculated by the ensemble average over all particles and configurations. Obviously, $\bar{Q}_{lm}$ as defined earlier is still dependent on the choice of reference frame. To obtain rotationally invariant equivalent parameters (Q_l), one needs to average over all m directions[28]:

$$Q_l = \sqrt{\frac{4\pi}{2l+1} \sum_{m=-1}^{l} |\bar{Q}_{lm}|^2} \quad (4)$$

In a noncrystalline liquid, the correlations dissipate rapidly, and values of Q_l tend to be small, with a value of 0 corresponding to absolute disorder, that is, a complete lack of any structural correlation (a situation corresponding to a disor-

Table 1. PEO–Oxygen/Li^+ Coordination and PEO Chain Conformations

System		O–Li Coordination		PEO Conformations[a]		
T (K)	N_{Li} (atoms)[b]	N^{o}_{coord} (atoms)[c]	ϕ^{o}_{coord} (%)[d]	ϕ^{tgt}_{triads} (%)	ϕ^{tgt}_{hexads} (%)	$\phi^{tgt}_{enneads}$ (%)
Nanoscopically confined PEO in Li^+ montmorillonite						
273	13	3.9	37	52	24	9
323	13	3.6	34	50	22	8
373	13	3.6	34	47	20	7
423	13	3.7	35	47	20	7
273	21	3.6	55	47	18	5
323	21	3.5	53	50	22	7
373	21	3.4	52	44	16	5
423	21	3.5	53	43	16	5
273	29	3.5	73	47	19	6
323	29	3.5	73	51	22	7
373	29	3.4	71	46	17	5
423	29	3.3	70	46	18	5
Bulk unconfined PEO with Li^+l^-						
273	8	6.2	12	69	43	25
298	8	6.2	12	68	41	24
323	8	6.3	12	66	40	21
373	8	6.3	12	61	34	16
398	8	6.1	12	57	29	14
423	8	6.1	12	53	25	11

[a] $\phi^{tgt}_{n\text{-seq}}$ is the fractions of ''helical'' dihedral n-sequences: triads (tgt), hexads ($tgttgt$), and enneads ($tgttgttgt$).
[b] N_{Li} is the number of Li^+ per montmorillonite layer for the nanoscopically confined systems, and the total number of Li^+ for the bulk PEO systems.
[c] N^{o}_{coord} is the number of PEO oxygens coordinated to each Li^+.
[d] ϕ^{o}_{coord} is the fraction (percentage) of coordinated PEO oxygens.

dered liquid). Most approaches employ only the Q_6 parameter as a "generic measure of crystallinity," since Q_6 is largely insensitive to any particular crystal symmetry. As for all Q_l, Q_6 is 0 for disordered states and increases in magnitude for more crystalline arrangements, where correlations through the structure develop.

RESULTS AND DISCUSSION

PEO–Li^+ Coordination

As will become obvious in the results and discussion following, the central physical factor—in addition to the effects of the severe geometric confinement—that determines the rest of the system properties is the PEO oxygen–Li^+ coordination. Here, we summarize at the outset the PEO–Li^+ coordination across the systems studied, and we shall later connect back to this data—as pertinent for the structural and dynamical properties discussed hereafter.

In Table 1, we tabulate for each system (T, N_{Li}) the number of ethylene-oxide oxygens that are coordinated to Li^+ (N^{O}_{coord}), derived by the integration of the first peak of the Li/PEO–oxygen pair distribution function (PDF) in the confined film. This number decreases with temperature (following approximately the respective Boltzmann factor for the coordination energy over kT) but remains more-or-less constant, about 3.5, across the various EO:Li ratios studied. This is a reasonable coordination number, given that the Li^+ spends the vast majority of time in the immediate vicinity of the SiO_2 surface of the montmorillonite[18] coordinated on average with 2.5 inorganic surface oxygens,[17] and thus can only coordinate with PEO oxygens in half of the space. This coordination behavior has as a direct consequence that as the EO:Li ratio is increased (for higher CEC, *i.e.*, higher N_{Li} per montmorillonite layer) an increasing fraction of the PEO oxygens is necessary to coordinate to all the Li cations. Specifically, for a typical montmorillonite CEC of 1.05 mequiv/g ($N_{Li} = 21$) about half the PEO oxygens

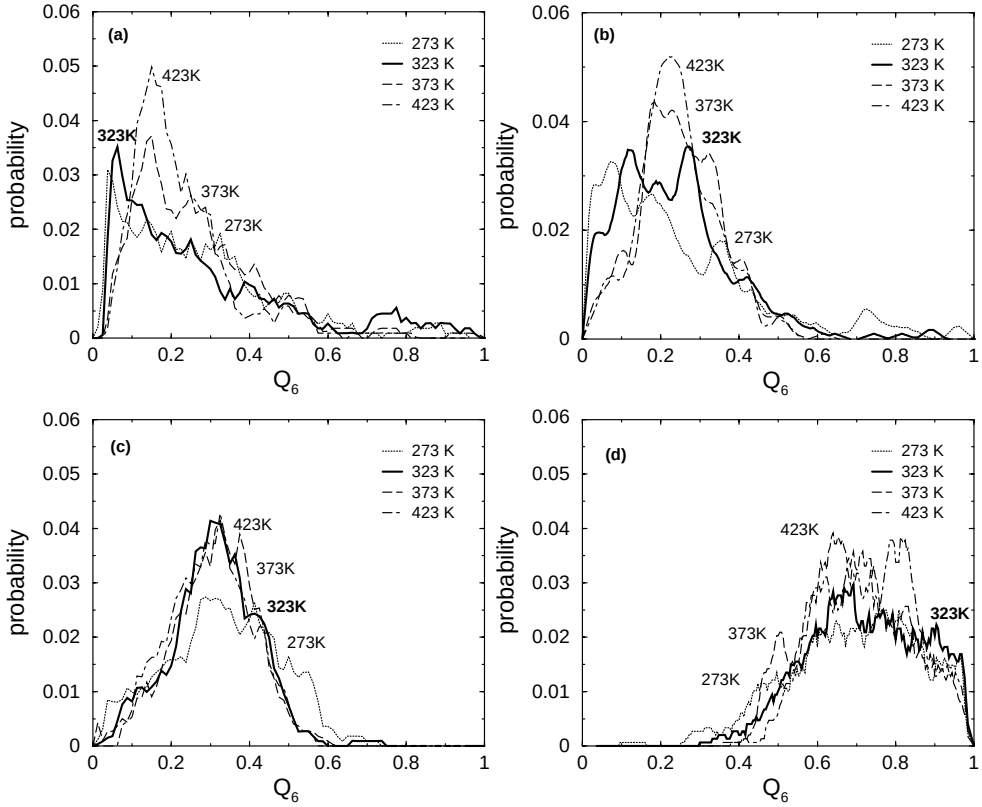

Figure 1. Distribution of rotationally invariant order parameters (Q_6) calculated for PEO/Li^+ thin films. Each figure corresponds to PEO intercalated in montmorillonite (MMT) with different CEC, that is, with different number of Li^+ per montmorillonite layer: (a) $N_{Li} = 29$ per simulated montmorillonite platelet, (b) $N_{Li} = 21$/MMT, (c) $N_{Li} = 13$/MMT, and (d) $N_{Li} = 0$/MMT.

are coordinated with a Li^+, whereas for a high CEC inorganic host (CEC = 1.44 mequiv/g, or N_{Li} = 29) about three quarters of the PEO oxygen are coordinated, and for a low CEC host (CEC = 0.64 mequiv/g, or N_{Li} = 13) only about a third of the PEO oxygens are coordinated with Li^+. For the bulk unconfined PEO/Li^+ systems, the oxygen–Li coordination numbers are about 6 for all temperatures studied, reflecting the fact that now there are no surface oxygens for Li^+ to coordinate with. This in turn results in temperature-independent fraction of coordinated PEO oxygen, which remains at a value of about 12%, reflecting the lower EO:Li ratio in these systems when compared with the confined ones.

Direct consequences of the PEO–Li coordination are manifested in the PEO chain conformations. Namely, the PEO oxygen–Li cation coordination necessitates a deviation from the lowest energy helical chain conformation, which is the chain conformation amenable to periodic stacking and thus crystal formation. More specifically, where dihedral angles along the chain backbones centered on a C—O bond adopt a trans (*t*) state and those centered on C—C bonds adopt gauche (*g*), crystallizable helical chain conformations are defined.[29] In Table 1, we tabulate such "crystallizable" PEO chain conformations through dihedral sequences across three (triads, —O—C—C—O— PEO segment, with a *tgt* helical conformation), six (hexads, —O—C—C— O—C—C—O— segment, with a *tgttgt* helical conformation), and nine dihedrals (enneads, —O—C—C—O—C—C—O—C—C—O— segment, with a *tgttgttgt* helical conformation). The fractions of specific dihedral sequences—PEO conformations—at each temperature were enumerated by directly counting the sequences' occurrence in the simulation ensembles. Comparing the PEO conformations in confinement *vs.* those in bulk PEO, we can see (a) a clear difference in relative numbers, with the PEO conformations in confinement having markedly lower popu-

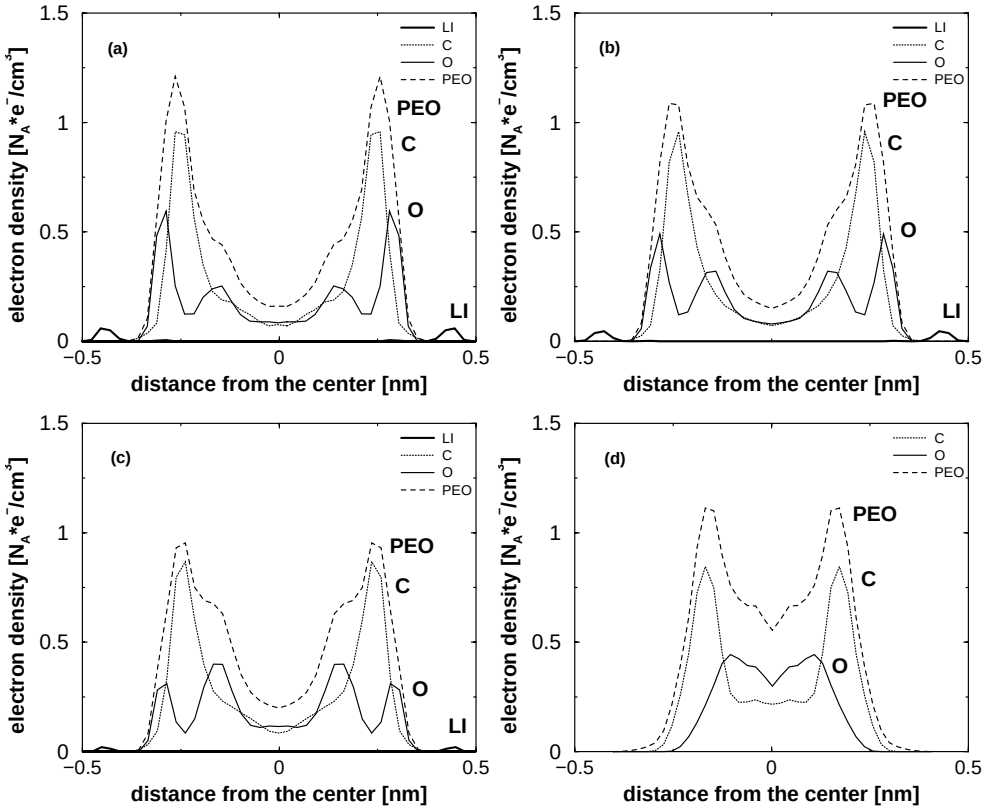

Figure 2. Electron density profiles of the various moieties across the slit pore for PEO/Li^+ thin films. The PEO is intercalated between confining surfaces of montmorillonite with different CEC, which corresponds to (a) $N_{Li} = 29$ Li^+ per montmorillonite platelet, (b) $N_{Li} = 21$/MMT, (c) $N_{Li} = 13$/MMT, and (d) $N_{Li} = 0$/MMT.

lations of helical structures (a direct consequence of the much higher oxygen–Li coordination in the confined systems and, to a lesser extent, confinement—geometric frustration—effects on the PEO conformations); and (b) a qualitative change with temperature for the bulk bearing signatures of a "melting" (as reported earlier, *cf.* Fig. 9 of a previous publication[19]), whereas in confinement PEO conformations only undergo the typical Boltzmann thermalization for each of the confined system.

Confined PEO Structure

As the CEC is varied across the simulated systems, a dramatic change is seen in the structure of PEO. These structural changes are probably best quantified through the distribution of the rotationally invariant order parameter, Q_6 (Fig. 1). As the number of lithium cations in the interlayer gallery decreases, the ensemble average value of the order parameter $\langle Q_6 \rangle$ (calculated over all the oxygen atoms of the PEO backbone) steadily increases. Thus, we see that the lesser the number of lithium ions in the system, the greater is the order between adjacent PEO chains. The underlying rationale behind such an effect is the strong coordination between the Li^+ and the oxygens of the PEO. This interaction forces the polymer chains to wrap around the Li^+, forming "crown-like" coordination structures. Thus, the polymer chains tend to exist in more "amorphous" conformations, rather than the ordered—semicrystalline—structure that is seen in bulk PEO. As the number of lithiums in the system increases, more oxygens take part in this coordination (*cf.* Table 1), further breaking-up any degree of order that they might possess. This hindrance to a regular arrangement of polymer chains is implicitly manifested by the low values of the rotationally invariant order parameter, Q_6. In the extreme case, where no Li^+ is present in the interlayer, the PEO adopts highly stretched configurations [Fig. 1(d)] dictated by the geometric constraints of the flat confining walls.

As the number of lithium ions present in the system changes, in addition to a quantitative var-

iation in the Q_6 mean value, there is also a qualitative change in the width of its distribution. As seen in Figure 1, the fewer Li^+ present, the narrower is the Q_6 distribution. This is because a change in the CEC of the system (corresponding to a change in the number of Li^+) directly influences the number of oxygens participating in coordination with the Li^+. Thus, with a greater number of Li^+ in the system, more of the PEO oxygens coordinate to the Li^+. However, at any given time, there are always some oxygens that are not coordinated to any lithium; thus, the presence of lithium leads to the oxygen atoms of the PEO finding themselves in an increasingly heterogeneous environment. Those PEO chains with their oxygens coordinated to the lithium are extremely disordered, and are represented by values of Q_6 close to 0. Those oxygens that are free are able to rearrange in some semblance of order, and therefore, display higher values of Q_6 (in the extreme case of no Li^+ in the system, Q_6 increases substantially in value). In this manner, the increase in lithium content is directly reflected in the increasing disorder of the PEO chains, as shown by the mean Q_6, and also represented by the increasing width of the Q_6 distributions.

This trend is also manifested in the structure of PEO across the confined film, as for example through the influence of CEC on the electron density profiles calculated perpendicular to the slit (in the direction of the z-axis). The confined PEO films correspond in all cases to a bilayer, that is, a film two monomers wide with a clearly developed layered structure, which is the most stable structure due to steric considerations.[30] However, the presence and population of Li^+ in the system strongly influence the density profiles of the PEO oxygens (Fig. 2), with a marked change in the shape of the profile that the rest of the PEO adopts across the confined film. Namely, due to the strong attraction with the negatively charged silicate wall, Li^+ ions are predominantly located in close proximity to the inorganic surfaces. In turn, because of their coordination with the lithium, a number of polymer oxygens are pulled toward the wall despite their partial negative charge. This effect forces some of the PEO oxygens to be located in the immediate vicinity of the solid surface, slightly closer to the wall than the covalently bonded carbons, and the rest of the oxygens belonging to the same chains are located on the other side of the density peak toward the center of the film. This gives rise to a "double oxygen bilayer" within the film, located on either

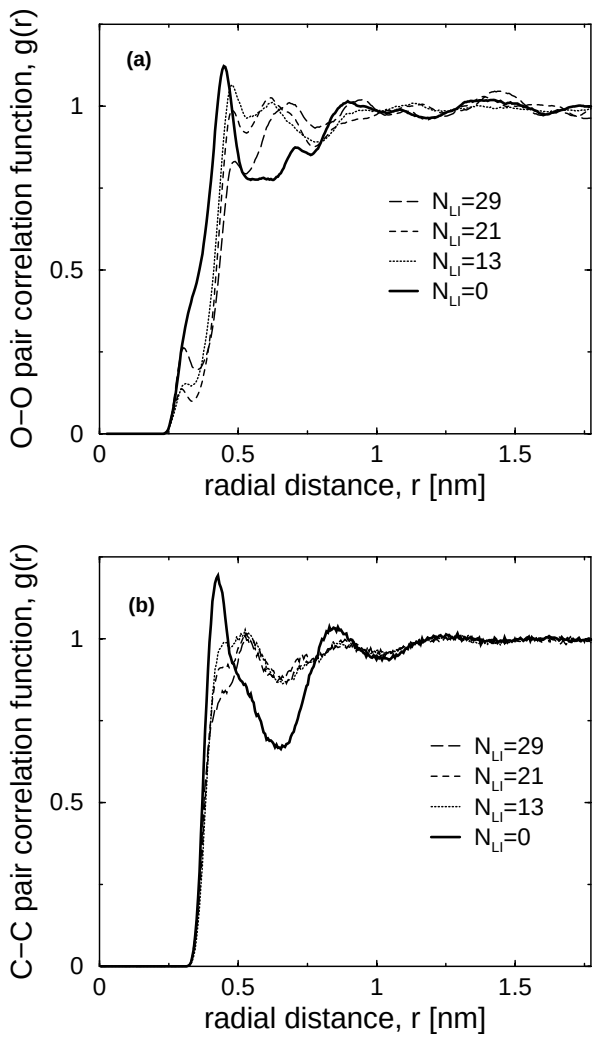

Figure 3. Interchain PDF calculated within a single slit in the confinement for (a) oxygen–oxygen pairs, and (b) carbon–carbon pairs. The various lines correspond to systems with montmorillonite of different CEC (as denoted by the N_{Li}). Note the influence of lithium on the first peak in the oxygen PDF, because of the O—Li coordination. This effect is less pronounced for the carbon PDF, since carbon atoms do not directly coordinate with the Li^+.

side of the carbon density peaks [Fig. 2(a–c)]. Decreasing the number of lithiums directly leads to a decrease in the number of the coordinated polymer oxygens immediately adjacent to the confining surface [*cf.* Fig. 2(a–c)]. An extreme example of this is the system in which there are no lithium present in the intergallery [Fig. 2(d)]; here, it is seen that the "double oxygen bilayer" completely disappears, with the density profile exhibiting only the characteristic twin peaks of a confined bilayer. This neutral system thus shows

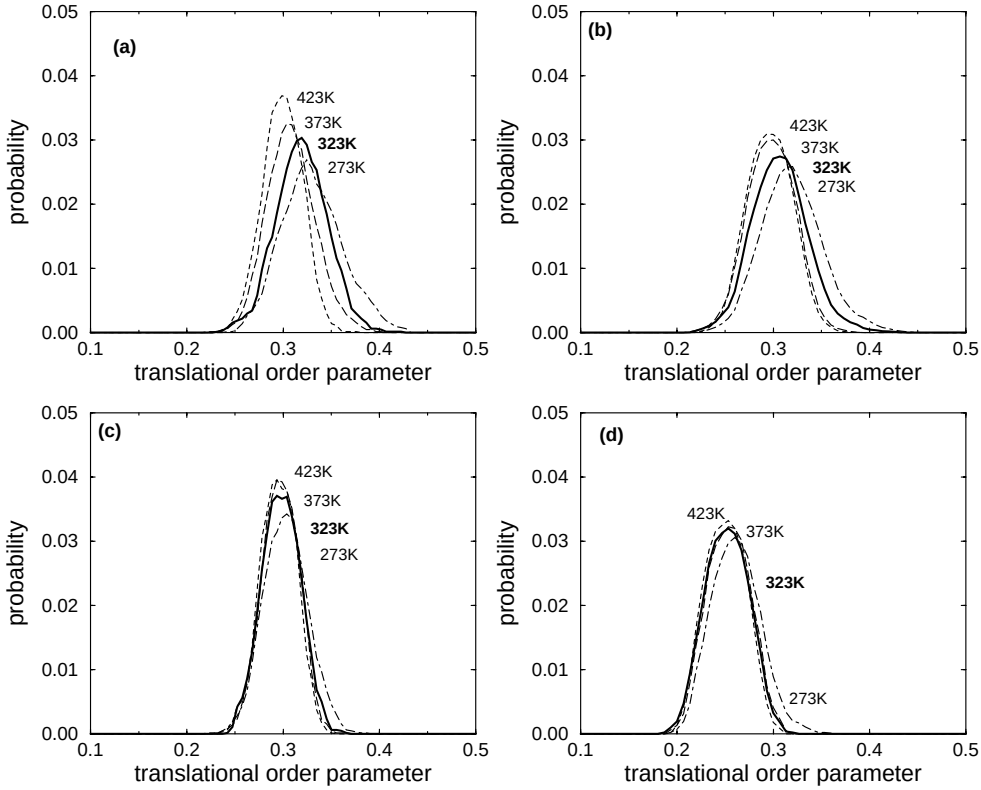

Figure 4. Distribution of translational order parameters calculated for interchain C—C pairs. PEO is intercalated between montmorillonites of varied CEC, which correspond to (a) $N_{Li} = 29$ Li^+ per montmorillonite platelet, (b) $N_{Li} = 21$/MMT, (c) $N_{Li} = 13$/MMT, and (d) $N_{Li} = 0$/MMT.

the most homogeneous density profile, a result that is also echoed by the high Q_6 values and narrower distributions for this system [Fig. 1(d)].

All the above behavior can be further illustrated by considering the interchain PDF [Fig. 3(a)]. For example, in the interchain oxygen PDF, the first peak becomes smaller with decreasing number of lithium ions in the system, eventually disappearing for the case in which there are no lithiums present in the confined film. To understand the origin of this first peak, one must again turn to the electron density profiles of Figure 2. The small first peak seen in PDFs of oxygen for high CEC values, at a distance of about 0.3 nm (Fig. 3), arises from the staggered oxygens present on either "side" of each carbon peak in the z-density bilayer, one toward the surface and one toward the center of the slit. As the number of lithiums in the system is decreased, the oxygen density peak immediately adjacent to the wall lowers in intensity, finally disappearing for the theoretical system corresponding to neutral walls. This behavior directly results in the lowering, and eventually the disappearance of the PDF peak at 0.3 nm, while there is a related simultaneous increase of the PDF peak at about 0.5 nm, which corresponds to the interchain oxygens within the same density layer that are not staggered normal to the confining surfaces. This simulation prediction, as quantified through the PDFs, can be directly tested experimentally by small-angle neutron scattering and total X-ray diffraction.[31,32]

Despite their high resolution in identifying order in the confined system, all the above quantities—Q_6, electron density profile, and PDFs—are structure-insensitive. Further elucidation of the manner in which order decreases in the system (as the number of Li^+ increases) can be provided by order parameters that probe specific structures and periodicities, such as the translational and orientational order parameters. For the systems with different CECs, the effect of the number of Li^+ ions on the carbon–carbon translational order parameter τ is different from that on the rotationally invariant order parameter, Q_6. In this case, it is seen that with decreasing number of lithiums, there is a slight decrease in the aver-

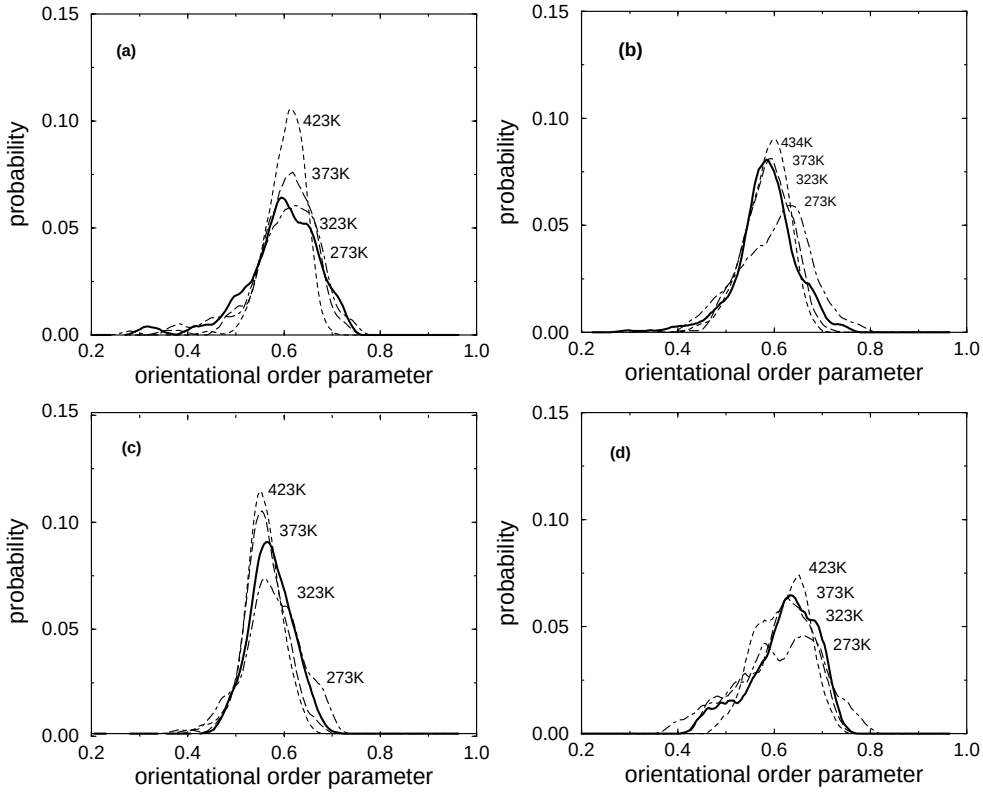

Figure 5. Distribution of orientational order parameters calculated for interchain oxygen quads. PEO is intercalated between montmorillonites of varied CEC, which correspond to (a) $N_{Li} = 29$ Li^+ per montmorillonite platelet, (b) $N_{Li} = 21$/MMT, (c) $N_{Li} = 13$/MMT, and (d) $N_{Li} = 0$/MMT.

age value, $\langle\tau\rangle$, and a narrowing of the τ distribution (Fig. 4). As with the Q_6, this behavior arises also from the interactions between the polymer and the lithium, albeit in an indirect manner: Li^+ and PEO carbons interact only via van der Waals forces and weak electrostatic repulsions (the PEO carbon has a positive partial charge); however, carbon atoms will bear signatures of structural changes with Li^+, since the oxygens—to which the carbons are covalently bonded along the chain—are influenced by the presence of a proximal/coordinated Li^+ (*cf.* Table 1). This is also evident in the interchain carbon–carbon PDF, as seen in Figure 3(b). As the number of Li^+ in the system decreases, the carbon interchain PDF becomes more homogeneous and well rounded, simply by virtue of the decreased coordination of oxygen with lithium, which dictates fewer oxygens in intimate contact with the confining surfaces. As mentioned earlier in eq 1, the distribution of τ is directly calculated from the individual interchain PDFs of all the carbon atoms in the system. Thus, with increasing number of Li^+, there is a greater deviation from a smooth PDF, which is consequently mirrored in the higher values of $\langle\tau\rangle$, indicating a slightly better carbon—and PEO chain—stacking within the layers as the lithium content increases.

Similarly, the distributions of oxygen orientational order parameter are also influenced by the number of lithium cations present (Fig. 5). The orientational order parameter q_i, as defined in eq 2, is calculated by considering the four nearest oxygen neighbors for each oxygen atom in the system. Since the presence of lithium promotes crown-ether type of arrangements around the Li^+, it leads to deviations from an oxygen tetrahedral arrangement, and thus promotes lower q_i structures. This behavior is manifested by increased heterogeneities in the oxygen structures, an effect readily visible in Figure 5(a–c), where the q_i distribution is seen to broaden with increasing numbers of Li^+ in the system. However, the average value $\langle q\rangle$ does not change appreciably, except for the extreme case where all lithium is removed from the system [Fig. 5(d)]. Thus, increasing lithium numbers in the system promote more diverse structures—higher struc-

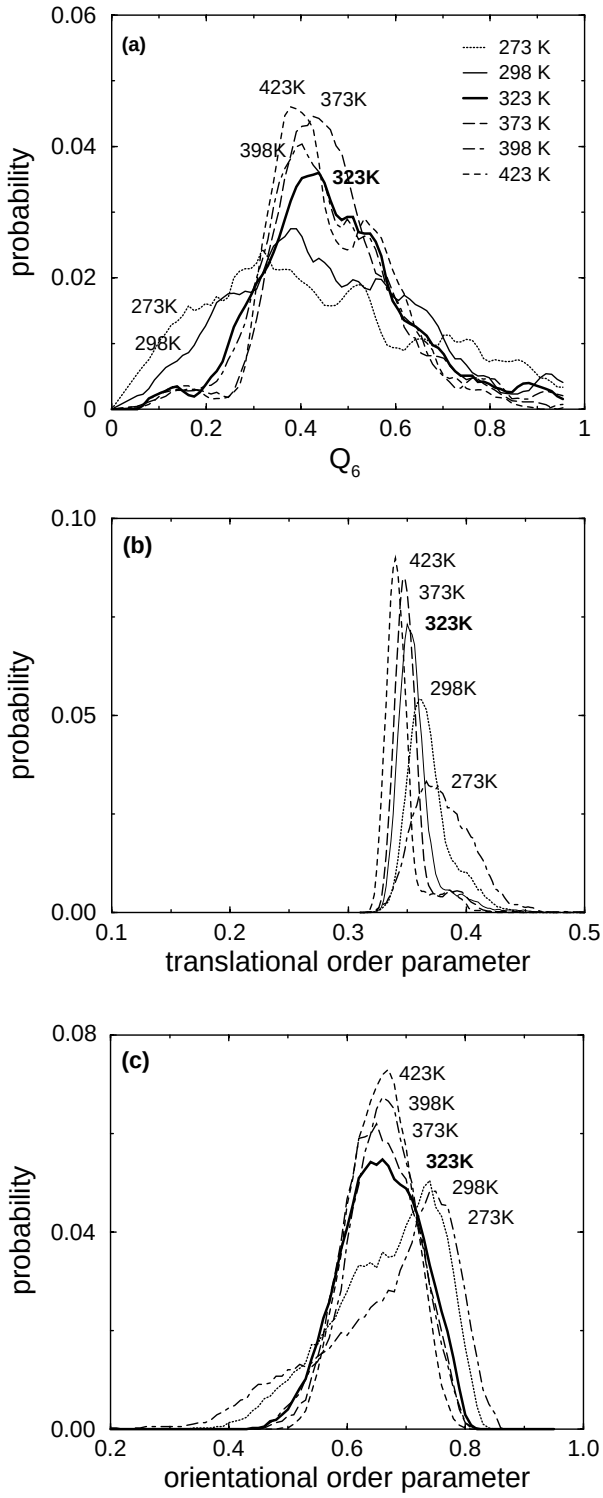

Figure 6. Distributions of three order parameters calculated for the bulk unconfined PEO/Li^+I^- system, as a function of temperature. A clear gradation in structural order is visible at about 323 K. (a) Rotationally invariant order parameter (Q_6), (b) carbon–carbon translational order parameter, and (c) oxygen orientational order parameter.

tural heterogeneity—for the oxygen tetrahedrals but do not induce a lower or higher oxygen tetrahedral order. In the extreme case, where all lithium is removed from the system, there develops a slightly stronger tetrahedral oxygen order, promoted by the absence of crown-ether PEO configurations; however, since the confined geometry between flat confining surfaces is not particularly commensurate with helical PEO structures (that would be characterized by high oxygen tetrahedral ordering and higher $\langle q \rangle$ values), the extent of this order increase remains small.

For Li^+ bearing confining montmorillonite surfaces, varying the CEC affects the structure of 1-nm thick confined PEO film. In summary, the greater the number of lithiums adjoining the surfaces (higher CEC), the greater the number of PEO oxygens coordinating with lithium, and the greater the heterogeneity in the oxygen structure (and by extension, the polymer configurations). Thus, more Li^+ leads to an increase in the confined system disorder, evidenced by a broadening in the distribution of all order parameters studied (Q_6, τ_i, and q_i) and a decrease in the mean value of the Q_6. However, it must be noted here that the disordering itself does not originate from the presence of lithium alone, but is primarily induced by the extreme dimensional restriction on the PEO in these almost two-dimensional systems. The effect of confinement is clearly demonstrated through the comparison against the same order parameters for the respective bulk unconfined PEO systems (Fig. 6), and is most perceptible in the temperature dependence of the conformational characteristics under confinement (Figs. 1, 4, and 5). Namely, although there is a slight change in the parameters of structural order with temperature under confinement, it is by far not as apparent as for the corresponding bulk systems (Fig. 6), where there is a qualitative and distinct change in order across 323 K. Even for the extreme case corresponding to the complete absence of any lithium in the confined systems, there is little change in any of the order parameters with temperature, suggesting that the structure (*i.e.* the extent of disorder in the system) remains at the same level throughout the temperatures studied. In contrast, for the bulk PEO system, there exists a clear gradation[33] in structure above a temperature close to the experimental melting point of bulk PEO [Fig. 6(a–c)]. All realistic nanoscopically confined systems exhibit higher disorder than the most disordered unconfined system simulated (at 423 K); a disor-

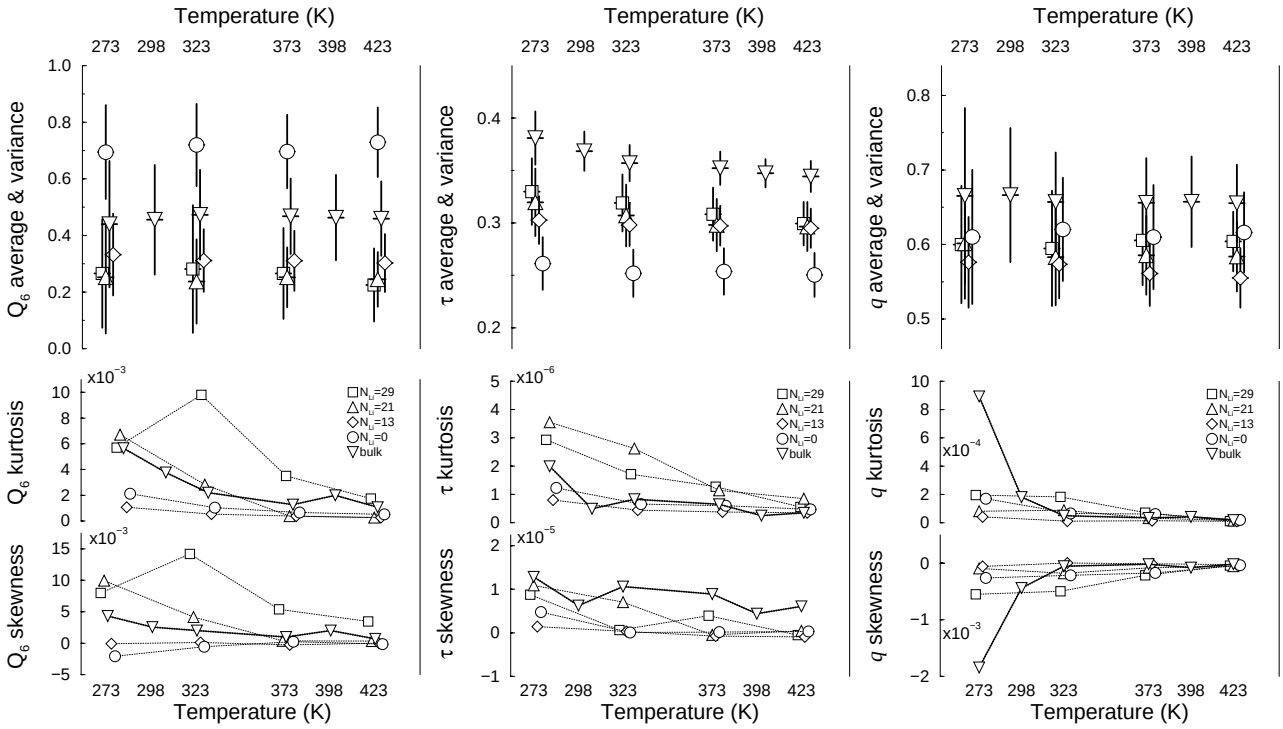

Figure 7. The first four moments of the probability distributions for the three order parameters studied (from left to right: Q_6, τ, and q). In the top panels, the first moment (average) is plotted as a symbol, and the square root of the second moment (variance) is plotted as a bar. In the bottom panels, the third (skewness) and fourth (kurtosis) moments are plotted as symbols, with lines connecting the various T-points for each system.

der which is developed because of the combined effects of the strong coordination of the PEO oxygens to the numerous Li^+ cations of the silicate surfaces (which promotes highly disordered, crown-like, conformations[34]) and of the severe (0.87-nm wide) geometric confinement between adjacent surfaces.

In addition to visually comparing the probability distributions of the three order parameters, it may be also informative to compare the moments of these distributions (Fig. 7). The standard definition for the moments of probability distributions is used, with the nth moment about the mean defined as[35] m_n:

$$m_n = \frac{\sum_{j=1}^{N}(x - x_j)^n p(x_j)}{\sum_{j=1}^{N} p(x_j)}, \quad n \geq 2; \quad \text{and} \quad \bar{x} = \frac{\sum_{j=1}^{N} x_j p(x_j)}{\sum_{j=1}^{N} p(x_j)} \tag{5}$$

where x is the variable—in our case the order parameters Q_6, τ, or q, respectively—with a mean value of $\bar{x}$ and a probability of $p(x_j)$ that the specific order parameter adopts a value x_j. The first moment ($\bar{x}$) corresponds to the mean value; the second moment ($n = 2$) is the variance, whose square root is the standard deviation; the third moment ($n = 3$) is the skewness of the distribution; and the forth moment ($n = 4$) is the kurtosis of the distribution. While the mean and the standard deviation are dimensional quantities, that is, have the same units as the measured quantities x_j, the skewness and the kurtosis are dimensionless. The skewness characterizes the degree of asymmetry of a distribution around its mean, whereas the kurtosis measures the relative "peakedness or flatness" of a distribution relative to the normal (Gaussian) distribution.

Upon comparison of the moments of the order parameter distributions between the bulk unconfined PEO and the nanoscopically confined—intercalated—PEO films (across varied EO:Li ratios and temperatures), we can derive the following conclusions (Fig. 7): From the first and second moments (Fig. 7, top panels): Despite the geometric confinement, all 1-nm thin PEO films are less ordered than the most disordered bulk unconfined PEO, across all temperatures studied.

This behavior occurs for all three of the order parameters studied—and across all EO:Li ratios considered—and reflects the highly disordered polymer conformations (*e.g.*, *tgt* dihedral triads/hexads, *etc*. *cf.*, Table 1) originating from the ethylene-oxide oxygen/Li coordination. As expected, in the system where PEO is confined between two solid surfaces in absence of any Li^+ cations, the rotationally invariant order parameter Q_6 is markedly larger than all other systems, reflecting the parallel to the confining-surfaces chain arrangement, and concurrently the parameter of translational order (τ) is respectively minimized. Secondly, increasing the number of lithium ions ($N_{Li} = 13, 21, 29$) increases the heterogeneity in the structure of PEO oxygens, as seen in the increase of the variance (*i.e.*, broadening of the distribution for all three of the order parameters calculated). Finally, although our PEO chains are too short to capture the genuine crystalline behavior of high molecular weight PEO, there exist clear traces of a melting transition in the bulk unconfined PEO systems. Most clearly, the parameter of orientational order (q) undergoes a qualitative change—in the mean value, skewness, and kurtosis—as T crosses 350 K. All confined systems show no such traces of a transition, and retain a highly amorphous (low means in all three parameters of order) structure throughout the temperature range simulated.

Dynamics

Lithium Diffusion

Simulation studies as well as experimental approaches have conclusively revealed that ionic conductivity and polymer chain dynamics are intimately connected in polymer–electrolyte/salt systems.[36,37] In the case of polymer/silicate nanocomposites, the massive silicate platelets act as the anionic component, whose immobilized negative charges are offset by the presence of mobile Li^+ cations. The intercalated polymer functions as the electrolyte and structural material. Our earlier studies[18] have shown the strong correlation between Li^+ dynamics and PEO backbone libration in the PEO/Li^+ montmorillonite system. It was seen that the balance of competing forces on the lithium, which is attracted both to the anionic silicate as well as to the partially charged oxygen moieties on the chain backbone, was responsible for the ubiquitous temperature-insensitive hopping mechanism for lithium ion dynamics.[18]

In systems with varying CEC, and thus varying lithium/oxygen ratios and varied montmorillonite/Li^+ attraction, the critical nature of the interplay of forces between Li^+ and PEO oxygen should be revealed, since it not only influences ion dynamics but also polymer chain relaxations. Because the lithium ions are coordinated to oxygens from adjacent polymer chains, and are also attracted to the wall surfaces, each individual cation acts as an effective "anchor" point, which binds polymer chains to the confining wall. The greater the number of charges present in the interlayer, the more organic oxygens participate in coordination, leading to greater extent of binding for the chains. At the same time, increasing the number of Li^+ also implies an increase of the inorganic negative charge per area (CEC), which leads to a greater binding strength for each lithium on the confining walls. Both these factors should lead to a decrease in the Li^+ mobility, with an increase in the number of Li^+ per montmorillonite (CEC), even in the absence of any Li^+/Li^+ steric or interaction mechanisms. This is reflected in the diffusion coefficients[38] for lithium motion in the interlayer confinement, which decrease with an increase in the number of lithium ions present in the system, as seen in Figure 8. At the same time, given the strong correlation between PEO dynamics and lithium mobility, where there are more Li^+ in the system (also characterized by decreased cation mobilities), there will also exist more extensive PEO coordination for a particular

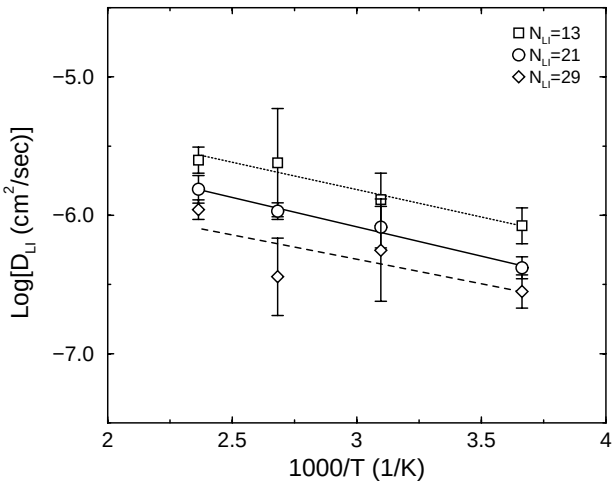

Figure 8. Diffusion coefficients for lithium, in PEO/Li^+ montmorillonite intercalates with varied CEC. Li^+ trajectories are primarily parallel to the confining walls, yielding MSD curves that are predominately Fickian over the timescale of the simulation.

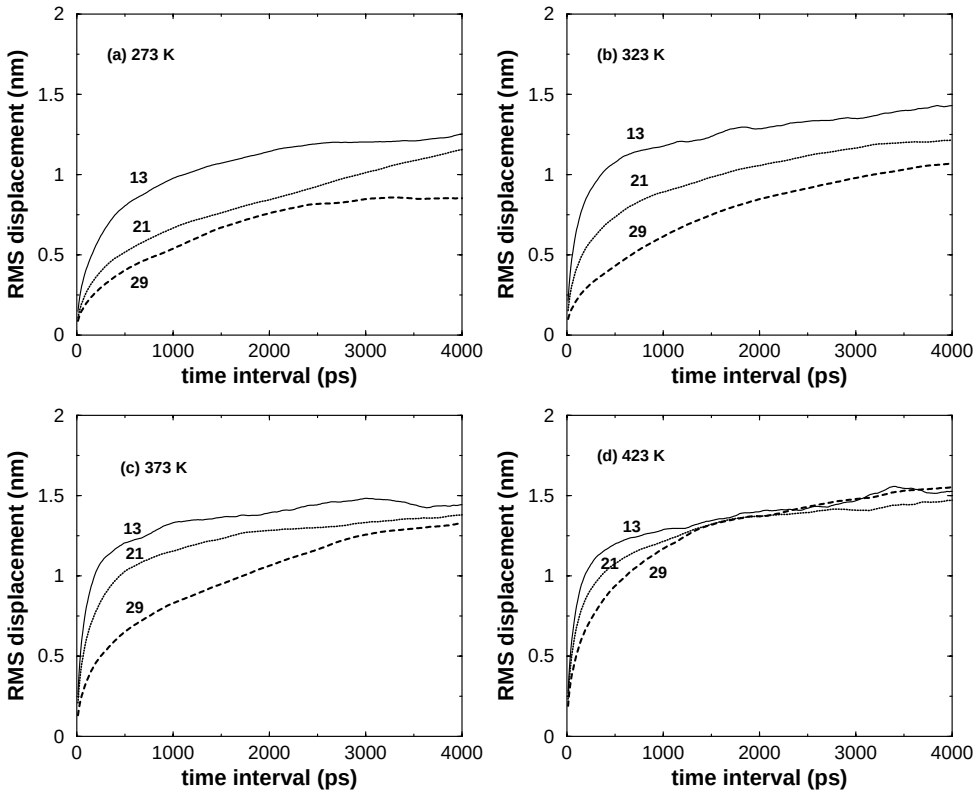

Figure 9. MSDs of PEO oxygens as a function of temperature: (a) 273 K; (b) 323 K; (c) 373 K; and (d) 423 K. The CEC of each system is denoted through the numbers of Li^+ per montmorillonite platelet.

chain, and thus it is expected that the more inhibited will be the PEO chain and segmental dynamics.[39] To the extent that activation energies can be calculated from these Li^+ diffusivities, all confined systems show a similar activation energy of about 7 kJ/mol. This activation energy is comparable to the one our simulations yield for the bulk PEO/Li^+ systems above 350 K (4 kJ/mol), and substantially lower than the activation energy for Li^+ in bulk PEO below 350 K (20 kJ/mol). This behavior captures the qualitative trends and the temperature dependence of Li^+ conductivities in intercalated systems and in bulk PEO.[10] Furthermore, considering the error associated with activation energy calculations both in simulations and in experiments, our simulations also reproduce the experimentally measured activation energies for Li^+ in intercalated systems and in amorphous bulk PEO (*ca.* 11 kJ/mol),[10] and are consistent for the bulk PEO at low (below 350 K) temperatures.

Finally, it may be informative to draw a parallel between our confined systems and those of a recent investigation of bulk PEO:$LiSbF_6$ complexes.[37] In that work, the authors observe that when the Li content is increased beyond a EO:Li ratio of 6:1, there develops ordering associated with Li-coordination structures, which is accompanied by high Li^+ mobilities.[37] This is clearly not happening in our confined systems (Figs. 7 and 8) despite having EO:Li ratios of 10.6:1, 6.5:1, and 4.7:1 (for $N_{Li} = 13$, 21, and 29, respectively). The increased crystalline ordering observed in the bulk PEO:$LiSbF_6$ systems, which is responsible for the dramatically increased Li^+ mobility, cannot be accommodated in Li^+ silicate intercalated geometries. Moreover, Li coordination in these confined systems is also with the oxygens of the montmorillonite surface, and this latter coordination—rather than the PEO:Li coordination—defines the mechanism of Li^+ motion.[18] In principle, if intercalation of PEO:$LiSbF_6$ were possible in Li^+ montmorillonite so as to achieve perfect helical PEO structures (*cf.* Fig. 1 of ref. 37), one could envision that similarly high lithium conductivities would also be achieved in the present intercalated systems.

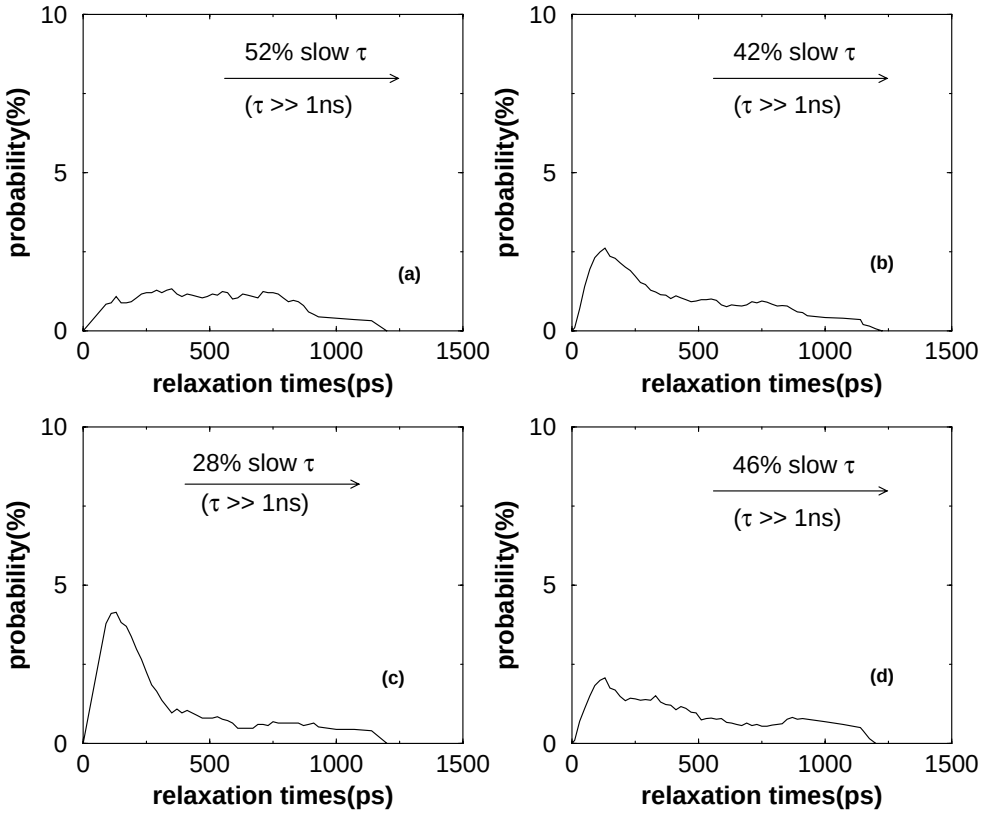

Figure 10. Distributions of fast and slow reorienting C—H moieties calculated for all C—H bonds in the system, at 273 K. The influence of the Li^+ is clearly visible when comparing across the various CEC, which correspond to (a) $N_{Li} = 29$ Li^+ per montmorillonite platelet, (b) $N_{Li} = 21$/MMT, (c) $N_{Li} = 13$/MMT, and (d) $N_{Li} = 0$/MMT.

PEO Chain Dynamics

The strong correlation between lithium ion and PEO dynamics was briefly mentioned in the previous section and was discussed in detail in earlier work.[18,19] This correlation, which arises because of the simultaneous coordination of the lithium to the wall and to the PEO oxygens, is also expected to have a concomitant effect on polymer dynamics. In Figure 9, the mean square displacements (MSD) for the polymer oxygens are shown as a function of time for the three different CEC studied, and across four different temperatures (273–423 K).

In all cases, it is evident that the presence of cationic charges has an effect on monomer motion, reflected in a decrease of the initial—almost linear—part of the MSD for the PEO oxygens in systems with larger numbers of Li^+ (higher CEC). This effect can be directly attributed to the pinning effect resulting from the electrostatic attraction between Li^+ and coordinated oxygens that belong to the montmorillonite and the PEO. This effective pinning results in the direct immobilization of any coordinated PEO oxygens, and through the chain connectivity an indirect immobilization of adjacent carbons and subsequent oxygens across the PEO chain. It is also seen that this effect becomes less pronounced with increasing temperature; since the potential barrier due to coordination energy is becoming easier to overcome by the kinetic energy at higher temperatures, and also because the Li^+ ions themselves are becoming more mobile, thus decreasing their anchoring efficacy. The effects of geometric confinement also become apparent in the oxygen MSD, through the typical change of slope as the oxygen explores spatial dimensions comparable with the confinement size; in Figure 9, this occurs at about 1.5 nm of RMS displacement for the higher temperatures (373–423 K) where all confined space can be explored, and at lower RMS displacements for the lower temperatures (273–323 K), where space is further restricted by immobilized chains pinned on the walls via Li coordination.

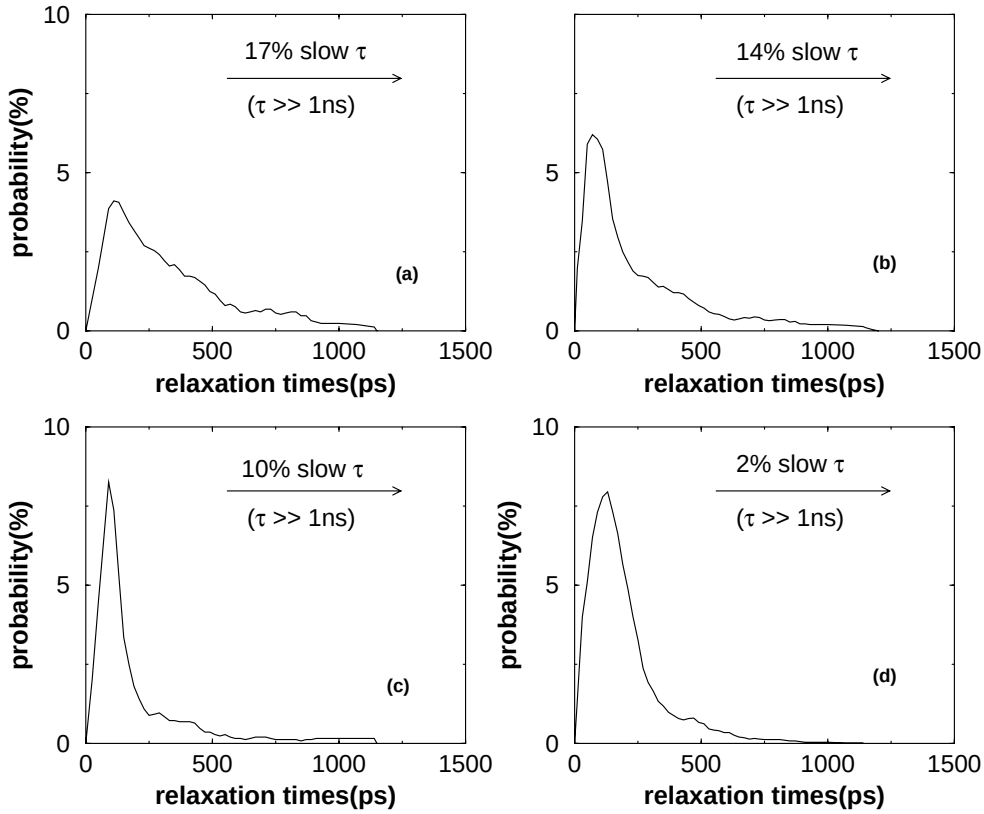

Figure 11. Distributions of fast and slow reorienting C—H moieties calculated for all C—H bonds in the system, at 423 K. The influence of the Li^+ is clearly visible when comparing across the various CEC, which correspond to (a) $N_{Li} = 29$ Li^+ per montmorillonite platelet, (b) $N_{Li} = 21$/MMT, (c) $N_{Li} = 13$/MMT, and (d) $N_{Li} = 0$/MMT.

Specifically, at long time scales, the logarithmic plot of oxygen MSDs *vs*. time shows a slope below 1. This deviation from classic diffusive behavior is a manifestation of the confined slit geometry, an effect that is also observed in computer simulations of the dynamics of supercooled chains close to their glass transition temperatures. In such studies,[40] the "caging" of monomers occurs also for finite times and yields a plateau in the log(MSD) *vs*. log(time) with a slope of 0.63. In the case of glasses, at long times, the monomers were observed to break free of their cages, and were able to establish classic Fickian diffusion with a slope of 1,[40] reflecting the dynamic nature of confinement in glass systems. In our case, however, the confinement restriction of the 1-nm slit does not relax with time. Hence, the free diffusive motion of polymer beads is permanently inhibited, and the long time slope remains smaller than 1. In contrast, our simulations of bulk unconfined PEO show oxygen MSDs with a slope close to 1 at longer time scales, reflecting the unhindered diffusive motion conventionally seen in the dynamics of bulk polymers. This contrasting behavior is also observed in a more dramatic fashion in the incoherent dynamic scattering functions calculated for bulk and confined polymers, in which the segmental dynamics of the bulk polymer exhibit homogeneous Gaussian displacements, while those of the confined polymer display dynamical heterogeneity with strong non-Gaussian characteristics.[41]

C—H Bond Reorientation

An indirect measure of PEO/Li^+ synergy is also found in the distribution of relaxation times for the reorientations of the C—H bond vectors of PEO. This quantity, although it may seem at first glance to be of less importance than the MSD, it is nevertheless worthwhile to discuss, since it is amenable to experimental investigation through solid-state NMR and dielectric spectroscopy studies[9,42,43] providing suitable properties for direct comparisons between the present MD simulations and experimental stud-

ies.[44,45] It was earlier shown[19] that the coexistence of fast and slow relaxation times for C—H bond vectors in these confined systems was indicative of dynamical heterogeneities arising from the presence of lithium, confinement-stabilized density fluctuations, and polymeric motion in the slit. The influence of lithium is clearly visible in Figures 10 and 11, in which the distributions of C—H reorientation relaxation times are shown. These relaxation times are determined from the MD simulations through analysis of the time autocorrelation functions of the C—H bond vectors (as detailed earlier[19]), and we quantify the distribution for motions with a characteristic relaxation time of less than 1 ns, whereas all slower relaxations are summarily grouped together and referred in the figures' inset text.

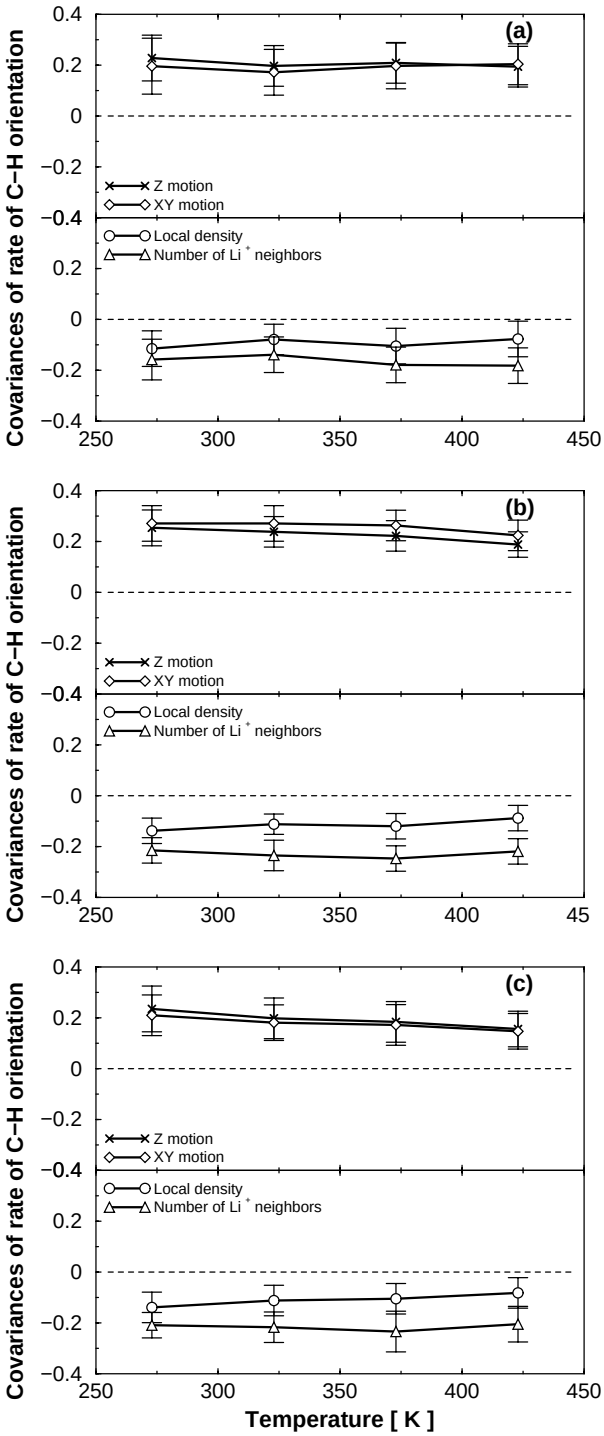

When comparing the behavior for the two temperatures shown, 273 K in Figure 10 and 423 K in Figure 11, it is evident that in both cases, there exist ultra-fast C—H reorientations with characteristic relaxation times of about 0.25 ns. These relaxations are only seen in these severely confined PEO systems and are absent in the respective bulk unconfined PEO; they have been, however, recently observed experimentally in quasi-elastic neutron scattering, and indirectly through dielectric relaxation spectroscopy, studies of PEO intercalated in montmorillonite,[46] and are strongly reminiscent of previous dielectric spectroscopy studies.[42] The population of these ultra-fast C—H modes is increasing with temperature (because of greater kinetic energy at higher temperatures), a behavior that is consistent with experimental results.[9] Finally, the persistence of slow C—H relaxations at the highest temperature for all realistic CECs [Fig. 11(a–c)] is another deviation from the bulk PEO behavior, which is also in concert with experimental observations of intercalated PEO systems.[9] This latter behavior is connected with the existence of Li^+ cations in the interlayer and the associated coordination of them to the PEO oxygens, as will be discussed shortly later, and as evident from the disappearance of all slow relaxing C—H bonds in confined systems with no Li^+ cations [Fig. 11(d)].

When systems with varied CEC and at different temperatures are compared [Fig. 10(a–c) *vs.* Fig. 11(a–c)], the changes in the distribution of fast and slow C—H moieties seem to be consistent

Figure 12. Influence of various physical factors on the relaxation rates of C—H bond reorientation, as represented by their covariances with the rates of reorientation of C—H bond vectors. In each case, the CECs of the adjacent confining surfaces are different, corresponding to (a) $N_{Li} = 29$ Li^+ per montmorillonite platelet, (b) $N_{Li} = 21$/MMT, and (c) $N_{Li} = 13$/MMT. In each panel, C—H bond reorientation is correlated with C—H bond translational motion normal (z) and parallel (xy) to the confining surfaces, with the local density around each C—H bond, and with number of adjacent Li^+.

with the changes in the coordinating Li^+ populations, and do not seem to indicate any qualitative changes in the mechanisms and the origins of the segmental relaxations. As discussed in length earlier,[19] the segmental PEO relaxations are correlated with various molecular mechanisms: specifically, fast C—H bond reorientations develop[19] (a) for segments that exhibit fast translational motions, normal or parallel to the surfaces; (b) for segments that are located in low local-density regions; and (c) for segments that have fewer than average adjacent Li^+ cations. These mechanisms were identified and their relative importance was quantified through calculations of the covariances between the instantaneous rate of C—H reorientation and the respective mechanisms (a–c above). To see whether there are any effects of the varied Li^+ number to the mechanisms responsible for the segmental PEO relaxations, we herewith undertake the same exercise of calculating the same four covariances as a function of varied CEC [Fig. 12(a–c)]. It is evident that within the simulation errors, there is no marked dependence of any of the covariances on the CEC of the system. For the covariances associated with translational motion and local-density, this behavior is probably expected, but for the covariance between the number of adjacent lithium next to a particular C—H unit and its rate of reorientation, it requires some explanation: This last covariance is about -0.2, and is maintained at a consistent level for all the systems, independent of the number of lithium present, and is hardly influenced by temperature (Fig. 12, open triangles). Firstly, by definition, these covariances are normalized for the number of Li^+ in each system, so it should not change simply because the number of lithiums is varied. However, we saw before that several structural and dynamic properties are sensitive to the CEC variations simulated, in particular, the distribution of C—H relaxation times. This last dependence is expected to change the value of the covariance to the extent that it changes the average rate of reorientation for the C—H moieties in the system, but ultimately it seems that is not sufficient to bring about an appreciable change in the value of the covariances. In conclusion, we see that the variation of the surface density of Li^+ (CEC) only changes the dynamics (absolute value of mobility) of the Li^+, whereas it does not markedly affect the mechanisms responsible for the confinement-induced dynamical behavior of the severely confined PEO chains.

CONCLUSIONS

Molecular dynamics computer simulations were used to study the effect of the CEC (surface density of Li^+) of montmorillonite on the structure and dynamics of severely confined PEO. It is seen that varying the surface density of Li^+ (CEC) quantitatively affects the PEO–oxygen/lithium coordination, and thus alters the polymer conformations in confinement. This effect is reflected in structural changes of the nanometer-thin confined PEO films as seen in the chain conformations, density profiles across the slit, PDFs, as well as the translational, orientational, and rotationally invariant order parameters. In particular, increasing the number of lithium ions increases the heterogeneity in the structure of PEO oxygens, implicitly seen in the broadening of the distribution for the order parameters calculated, and in the chain conformations. These effects are in addition to the confinement-induced disorder in these systems, which (unlike bulk PEO) does not show a distinct change from solid-like to liquid-like features with temperature. The influence of the CEC is also apparent in the dynamic response of the system: a decrease in the number of lithium leads to an increase in the diffusion coefficients of Li^+, and a change in the distribution of relaxation rates for C—H bond reorientation. However, changes in the CEC do not seem to alter the origins of the confinement-induced dynamics in these systems.

This project was partly supported by ACS/PRF (PRF grant No. 37,274-G5), and computational resources were provided through the "Materials Simulation Center" (a Penn-State Center for Nanoscale Science (MRSEC-NSF) and MRI facility) and by IGERT (NSF-DGE grant 9987589). For the duration of this work, EM was a recipient of the "Virginia S. and Philip L. Walker Jr." endowment faculty fellowship. We are grateful to Ramanan Krishnamoorti (U. Houston) and David Zax (Cornell) for fruitful discussions, and the anonymous reviewers for valuable suggestions.

REFERENCES AND NOTES

1. Giannelis, E. P.; Krishnamoorti, R.; Manias, E. Adv Polym Sci 1999, 138, 107.
2. Vaia, R. A. In Polymer-Clay Nanocomposites; Pinnavaia, T. J.; Beall, G. W., Eds.; Wiley: New York, 2001; p 229.
3. Wang, L.; Rocci-Lane, M.; Brazis, P.; Kannewurf, C. R.; Kim, Y.; Lee, W.; Choy, J.; Kanatzidis, M. G. J Am Chem Soc 2000, 122, 6629.

4. Wang, L.; Kanatzidis, M. G. Chem Mater 2001, 13, 3717.
5. Liu, Y. J.; Schindler, J. L.; DeGroot, D. C.; Kannewurf, C. R.; Hirpo, W.; Kanatzidis, M. G. Chem Mater 1996, 8, 525.
6. Alexandre, M.; Dubois, P. Mater Sci Eng R Rep 2000, 28, 1.
7. Vaia, R. A.; Sauer, B. B.; Tse, O. K.; Giannelis, E. P. J Polym Sci Part B: Polym Phys 1997, 35, 59.
8. Aranda, P.; Ruiz-Hutsky, E. Chem Mater 1992, 4, 1395.
9. Wong, S.; Vaia, R. A.; Giannelis, E. P.; Zax, D. B. Solid State Ionics 1996, 86, 547.
10. Vaia, R. A.; Vasudevan, S.; Krawiec, W.; Scanlon, L. G.; Giannelis, E. P. Adv Mater (Weinheim, Ger) 1995, 7, 154.
11. Wu, J.; Lerner, M. M. Chem Mater 1993, 5, 835.
12. Theng, B. K. G.; Hayashi, S.; Soma, M.; Seyama, H. Clays Clay Miner 1997, 45, 718.
13. Bujdak, J.; Komadel, P. J Phys Chem B 1997, 101, 9065.
14. Bujdak, J.; Janek, M.; Madelova, J.; Komadel, P. Clays Clay Miner 2001, 49, 244.
15. Bujdak, J.; Hackett, E.; Giannelis, E. P. Chem Mater 2000, 12, 2168.
16. Yang, D. K.; Zax, D. B. J Chem Phys 1999, 110, 5325.
17. Hackett, E.; Manias, E.; Giannelis, E. P. Chem Mater 2000, 12, 2161.
18. Kuppa, V.; Manias, E. Chem Mater 2002, 14, 2171.
19. Kuppa, V.; Manias, E. J Chem Phys 2003, 118, 3421.
20. Kuppa, V.; Menakanit, S.; Krishnamoorti, R.; Manias, E. J Polym Sci Part B: Polym Phys 2003, 41, 3285.
21. Berendsen, H. J. C.; Postma, J. P. M.; van Gunsteren, W. F.; DiNola, A.; Haak, J. R. J Chem Phys 1984, 81, 3684.
22. In reality, the negative charges of the montmorillonite layer originates from defects—mostly in the octahedral trivalent-Al positions, which are isomorphically substituted by divalent metals (such as Mn and Fe). In our montmorillonite model, we do not define explicit defect sites, rather we smeared the defect charge equally to all Al sites in the silicate lattice. For details and models that explicitly account for such lattice defents, one can refer to other literature, for example, to a recent article by Heinz and Suter (see ref. 23) and references therein.
23. Heinz, H.; Suter, U. W. J Phys Chem B 2004, 108, 18341.
24. Theng, B. K. G. Formation and Properties of Clay Polymer Complexes; Elsevier: New York, 1979.
25. Errington, J. R.; Debenedetti, P. G. Nature 2001, 409, 318.
26. Chau, P. L.; Hardwick, A. J. Mol Phys 1998, 93, 511.
27. Steinhardt, P. J.; Nelson, D. R.; Ronchetti, M. Phys Rev B: Condens Matter 1983, 28, 784.
28. ten Wolde, P. R.; Ruiz-Montero, M. J.; Frenkel, D. J Chem Phys 1996, 104, 9932.
29. Neyertz, S.; Brown, D.; Thomas, J. O. J Chem Phys 1994, 101, 10064.
30. Israelachvili, J. Intermolecular and Surface Forces; Academic Press: London, 1991.
31. Trikalitis, P. N.; Petkon, V.; Kanatzidis, M. G. Chem Mater 2003, 15, 3337.
32. Petkon, V.; Trikalitis, P. N.; Bozin, E. S.; Billinge, J. L.; Vogt, T.; Kanatzidis, M. G. J Am Chem Soc 2002, 124, 10157.
33. A clear gradation in structure is captured for the bulk—unconfined—systems by the order parameters studied here as the temperature increases above 323 K, despite the relatively short length of the simulated PEO chains, which are not expected to develop genuine crystalline structures even for the unconfined/bulk systems. This behavior stems from the fact that the order parameters defined here are highly sensitive to local/interatomic structures, and are not purely a measure of long-range order in the systems.
34. Strawhecker, K.; Manias, E. Chem Mater 2003, 15, 844.
35. McQuarie, D. A. Statistical Mechanics; University Science Books: Herndon, VA, 2000; p 20.
36. Muller-Plathe, F.; van Gunsteren, W. F. J Chem Phys 1995, 103, 4745.
37. Gadjourova, Z.; Andreev, Y. G.; Tunstall, D. P.; Bruce, P. G. Nature 2001, 412, 520.
38. The diffusion coefficients shown in Figure 8 were calculated from the slopes of mean square displacement curves, which look Fickian in form throughout the simulated time interval of 5 ns, and correspond to hopping cation motions as discussed in previous work (see ref. 18).
39. Smith, G. D.; Jaffe, R. L.; Yoon, D. Y. J Phys Chem 1993, 97, 12752.
40. Varnik, F.; Baschnagel, J.; Binder, K. Eur Phys J E Soft Matter 2002, 8, 175.
41. Kuppa, V.; Zax, D. B.; Manias, E. Phys Rev Lett, submitted for publication.
42. Anastasiadis, S. H.; Karatasos, K.; Vlachos, G.; Giannelis, E. P.; Manias, E. Phys Rev Lett 2000, 84, 915.
43. Jin, X.; Zhang, S. H.; Runt, J. Polymer 2002, 43, 6247.
44. Manias, E.; Kuppa, V.; Yang, D. K.; Zax, D. B. Colloid Surf A 2001, 187, 509.
45. Manias, E.; Kuppa, V. Eur Phys J E Soft Matter 2002, 8, 193.
46. Anastasiadis, S. H.; Afratis, A.; Chrissopoulou, K.; Giannelis, E. P.; Frick, B, private communications.